

Multi-Channel Selective Femtosecond Coherent Control Based on Symmetry Properties

Andrey Gandman, Lev Chuntunov, Leonid Rybak and Zohar Amitay*

Schulich Faculty of Chemistry, Technion - Israel Institute of Technology, Haifa 32000, Israel

Abstract

We present and implement a new scheme for extended multi-channel selective femtosecond coherent control based on symmetry properties of the excitation channels. Here, an atomic non-resonant two-photon absorption channel is coherently incorporated in a resonance-mediated (2+1) three-photon absorption channel. By proper pulse shaping, utilizing the invariance of the two-photon absorption to specific phase transformations of the pulse, the three-photon absorption is tuned independently over order-of-magnitude yield range for any possible two-photon absorption yield. Noticeable is a set of "two-photon dark pulses" inducing widely-tunable three-photon absorption.

PACS numbers: 32.80.Qk, 32.80.Wr, 42.65.Re

*Electronic address: amitayz@tx.technion.ac.il

When a quantum system is irradiated with a broadband femtosecond pulse, a coherent manifold of quantum pathways is photo-induced from one state to the other. Shaping the pulse [1] to manipulate the interferences among these pathways is the means by which femtosecond coherent control affects state-to-state transition probabilities [2, 3, 4, 5, 6]. When several excitation channels to different final states of the system are of concern, in many cases it is sufficient to achieve basic multi-channel selective control ("on-off" type) of maximizing one channel while minimizing the other channels. However, in many other cases a much higher degree of selectivity is desirable, where ideally one channel is tuned independently over its full yield range while the other channels are set constant on any chosen possible yields. This requires pulse shapes that reduce the correlations between the different channel yields.

Such extended multi-channel selective femtosecond control have been experimentally studied so far mostly by employing automatic "black-box" optimization of the pulse shape using learning algorithms [7, 8, 9, 10]. Here we focus on rational femtosecond coherent control, where the pulse shaping is based on identifying first the state-to-state interfering pathways and their interference mechanism. By itself rational femtosecond control is suitable mainly to quantum systems of limited complexity, however it might also serve as a basis for establishing control principles that will be incorporated in extended control schemes of high-complexity systems. To date, the only rational femtosecond control work studied aspects of extended multi-channel selective control is the one by Dudovich *et al.* [11] on polarization control of two-photon absorption to different angular-momentum states. All the other past studies of rational selective femtosecond control involve the simpler ("on-off") scheme [12, 13, 14].

In this Letter we present and demonstrate a new rational scheme for extended multi-channel selective femtosecond coherent control that is based on symmetry properties of the excitation channels. The processes under study here are multiphoton absorption processes that are of fundamental and applicative importance and have been shown to be coherently controlled very effectively [6, 11, 13, 14, 15, 16, 17, 18, 19, 20, 21, 22, 23, 24, 25, 26, 27]. The present atomic scenario involves a non-resonant two-photon absorption channel that is coherently incorporated in a resonance-mediated (2+1) three-photon absorption channel. Their one-channel control have previously been studied separately [15, 24]. Here, by utilizing a symmetry property of the two-photon absorption for proper pulse shaping, the three-photon

absorption is tuned independently over order-of-magnitude yield range for any possible yield of the two-photon absorption. The approach developed here is general, conceptually simple, and very effective.

The two-channel excitation considered here is shown schematically in Fig. 1. It involves an initial ground state $|g\rangle$ and two excited states $|f_1\rangle$ and $|f_2\rangle$. The $|g\rangle$ and $|f_1\rangle$ states are coupled by a non-resonant two-photon coupling provided by a manifold of states $|v\rangle$ that are far from resonance. The $|f_1\rangle$ and $|f_2\rangle$ states are coupled resonantly by one-photon coupling. Hence, when irradiated with a weak (shaped) femtosecond pulse a non-resonant two-photon absorption from $|g\rangle$ to $|f_1\rangle$ is induced simultaneously with a resonance-mediated (2+1) three-photon absorption from $|g\rangle$ to $|f_2\rangle$ with $|f_1\rangle$ as an intermediate state. The final (complex) amplitudes A_{f_1} and A_{f_2} of states $|f_1\rangle$ and $|f_2\rangle$ after the pulse is over are given, respectively, by 2nd- and 3rd-order time-dependent perturbation theory as [15, 24]

$$A_{f_1} = -\frac{1}{i\hbar^2} \mu_{f_1,g}^2 A^{(2)}(\omega_{f_1,g}), \quad (1)$$

and

$$A_{f_2} = \frac{1}{\hbar^3} \mu_{f_2,f_1} \mu_{f_1,g}^2 \left[A_{f_2}^{(2+1)on-res} + A_{f_2}^{(2+1)near-res} \right], \quad (2)$$

$$A_{f_2}^{(2+1)on-res} = i\pi E(\omega_{f_2,f_1}) A^{(2)}(\omega_{f_1,g}), \quad (3)$$

$$A_{f_2}^{(2+1)near-res} = -\wp \int_{-\infty}^{\infty} \frac{1}{\delta} A^{(2)}(\omega_{f_1,g} - \delta) E(\omega_{f_2,f_1} + \delta) d\delta, \quad (4)$$

with

$$A^{(2)}(\Omega) = \int_{-\infty}^{\infty} E(\omega) E(\Omega - \omega) d\omega = \int_{-\infty}^{\infty} E(\Omega/2 - \alpha) E(\Omega/2 + \alpha) d\alpha. \quad (5)$$

The quantities μ_{f_2,f_1} and $\mu_{f_1,g}^2$ are, respectively, the $|f_2\rangle$ - $|f_1\rangle$ one-photon dipole matrix element and $|f_1\rangle$ - $|g\rangle$ effective non-resonant two-photon dipole coupling [15], and $\omega_{m,n}$ is the transition frequency between a pair of states. The $E(\omega) \equiv |E(\omega)| \exp[i\Phi(\omega)]$ is the pulse spectral field, related to the temporal field by Fourier transform, with $|E(\omega)|$ and $\Phi(\omega)$ being, respectively, the spectral amplitude and phase of frequency ω . For the (unshaped) transform-limited pulse, which is the shortest pulse for a given spectrum $|E(\omega)|$, $\Phi(\omega) = 0$ for any ω . The final populations of $|f_1\rangle$ and $|f_2\rangle$ are given, respectively, by $P_{f_1} = |A_{f_1}|^2$ and $P_{f_2} = |A_{f_2}|^2$. They serve as the measures for the two-photon and three-photon absorption.

The final amplitude A_{f_1} of $|f_1\rangle$ coherently interferes all the possible non-resonant two-photon pathways from $|g\rangle$ to $|f_1\rangle$, i.e., coherently integrates over all their corresponding

amplitudes. Each such pathway is composed of two absorbed photons of frequencies ω and $\omega_{f_1,g} - \omega$. The final amplitude A_{f_2} of $|f_2\rangle$ coherently interferes all the possible resonance-mediated (2+1) three-photon pathways from $|g\rangle$ to $|f_2\rangle$. Each such pathway is either on resonance or near resonance with $|f_1\rangle$, having a corresponding detuning δ . It involves a non-resonant absorption of two photons with a two-photon transition frequency $\omega_{f_1,g} - \delta$ and the absorption of a third complementary photon of frequency $\omega_{f_2,f_1} + \delta$. The term $A_{f_2}^{(2+1)on-res}$ interferes all the on-resonant pathways ($\delta = 0$), while the term $A_{f_2}^{(2+1)near-res}$ interferes all the near-resonant pathways ($\delta \neq 0$) with a $1/\delta$ amplitude weighting. The on-resonant pathways are excluded from $A_{f_2}^{(2+1)near-res}$ by the Cauchy's principal value operator \wp . Several two- and three-photon pathways are shown schematically in Fig. 1. The different amplitudes are expressed using the parameterized amplitude $A^{(2)}(\Omega)$ interfering all the possible two-photon pathways with transition frequency Ω , each composed of two photons with frequencies ω and $\Omega - \omega$, or, equivalently, $\Omega/2 - \alpha$ and $\Omega/2 + \alpha$, i.e., two frequencies located symmetrically around $\Omega/2$. The amplitudes A_{f_1} and $A_{f_2}^{(2+1)on-res}$ are proportional to $A^{(2)}(\Omega = \omega_{f_1,g})$, while $A_{f_2}^{(2+1)near-res}$ integrates over all the $A^{(2)}(\Omega = \omega_{f_1,g} - \delta)$ with non-zero detuning ($\delta \neq 0$).

In order to achieve high degree of selectivity between the two- and three-photon absorption channels we utilize phase transformations $\hat{U}_{\text{phase}}^{(\text{selective-cntrl})}$ of the spectral field $E(\omega)$ that do not change the two-photon absorption amplitude A_{f_1} but do change the three-photon absorption amplitude A_{f_2} . Based on Eqs. (1)-(5), it applies to any transformation

$$\hat{U}_{\text{phase}}^{(\text{selective-cntrl})} = \exp[i\Delta\Phi_{\text{antisym}}(\omega)] \quad (6)$$

that corresponds to the addition of a spectral phase pattern $\Delta\Phi_{\text{antisym}}(\omega) \equiv \Delta\Phi_{\text{antisym}}(\omega_{f_1,g}/2 + \alpha)$ that is anti-symmetric around $\omega_{f_1,g}/2$, i.e., for any value of α it satisfies the relation

$$\Delta\Phi_{\text{antisym}}(\omega_{f_1,g}/2 + \alpha) = -\Delta\Phi_{\text{antisym}}(\omega_{f_1,g}/2 - \alpha) . \quad (7)$$

Such phase addition keeps the value of $A^{(2)}(\Omega = \omega_{f_1,g})$ unchanged, while it generally changes the value of $A^{(2)}(\Omega = \omega_{f_1,g} - \delta)$ for $\delta \neq 0$. Hence, it alters A_{f_2} while keeping A_{f_1} invariant.

So, the following extended selective coherent control scheme for designing the spectral phase pattern $\Phi(\omega)$ can be applied: The two-photon absorption amplitude A_{f_1} is set to a chosen value $A_{f_1,\text{base}}$ by choosing a proper base phase pattern $\Phi_{\text{base}}(\omega)$. Then, by adding different suitable anti-symmetric phase patterns $\Delta\Phi_{\text{antisym}}(\omega)$, the three-photon absorption

amplitude A_{f_2} is tuned from its base value $A_{f_2,\text{base}}$ over a wide range of values, while A_{f_1} is kept constant on $A_{f_1,\text{base}}$. The total spectral phase pattern applied to the shaped pulse is $\Phi(\omega) = \Phi_{\text{base}}(\omega) + \Delta\Phi_{\text{antisym}}(\omega)$.

The phase patterns chosen here as $\Phi_{\text{base}}(\omega)$ and $\Delta\Phi_{\text{antisym}}(\omega)$ are shown schematically in Fig. 1. The present base patterns $\Phi_{\text{base}}(\omega)$ are of a single π step at variable position $\omega_{\text{step}}^{\text{base}}$. As previously shown [15], this family of pulse shapes allows high degree of the control over the full range of the non-resonant two-photon absorption channel. It ranges from zero absorption, corresponding to "two-photon dark pulses", up to the maximal possible absorption, corresponding to the TL pulse that induces fully constructive interferences among all the two-photon pathways [see Eqs.(1) and (5)]. In other separate studies [24], the π -step patterns have also been shown to be very effective in controlling the resonance-mediated (2+1) three-photon absorption channel. The present anti-symmetric phase additions $\Delta\Phi_{\text{antisym}}(\omega)$ are composed of two steps of variable amplitude $\Phi_{\text{amp}}^{\text{antisym}}$ positioned symmetrically around $\omega_{f_1,g}/2$ at variable positions that are represented by the left-step position $\omega_{\text{left-step}}^{\text{antisym}}$.

The physical model system of the study is the sodium (Na) atom [28], with the $3s$ ground state as $|g\rangle$, the $4s$ state as $|f_1\rangle$, and the $7p$ state as $|f_2\rangle$ (see Fig. 1). The transition frequency $\omega_{f_1,g} \equiv \omega_{4s,3s} = 25740 \text{ cm}^{-1}$ corresponds to two 777-nm photons and the transition frequency $\omega_{f_2,f_1} \equiv \omega_{7p,4s} = 12801 \text{ cm}^{-1}$ corresponds to a 781.2-nm photon. The $3s$ - $4s$ non-resonant two-photon coupling originates from the manifold of p -states, particularly from the $3p$ state [$\omega_{3p,3s} \sim 16978 \text{ cm}^{-1}$ (589 nm)]. The sodium is irradiated with phase-shaped linearly-polarized femtosecond pulses having a Gaussian intensity spectrum centered around 780 nm (12821 cm^{-1}) with 5.8-nm (95-cm^{-1}) bandwidth ($\sim 180\text{-fs}$ TL duration).

Experimentally, a sodium vapor in a heated cell is irradiated with such laser pulses, after they undergo shaping in an optical setup incorporating a pixelated liquid-crystal spatial light phase modulator [1]. The effective spectral shaping resolution is $\delta\omega_{\text{shaping}} = 2.05 \text{ cm}^{-1}$ per pixel. The peak intensity of the TL pulse is below 10^9 W/cm^2 . Following the interaction with a pulse, the population excited to the $4s$ state radiatively decays to the lower $3p$ state, which then decays to the $3s$ ground state. The $3p$ - $3s$ fluorescence serves as the relative measure for the total $4s$ population $P_{f_1} \equiv P_{4s}$. The population excited to the $7p$ state undergoes radiative and collisional decay to lower excited states, including the $4d$, $5d$, $6d$, and $6s$ states. The fluorescence emitted in their decay to the $3p$ state serves as the relative measure for the total $7p$ population $P_{f_2} \equiv P_{7p}$. The fluorescence is measured using a spectrometer coupled

to a time-gated camera system. The $3p$ - $3s$ fluorescence part originating from the $4s$ state is discriminated from the part originating from the $7p$ state by using a proper detection gate width, utilizing the different time scales of the $4s$ -to- $3p$ and $7p$ -to- $3p$ decays.

Figure 2(a) presents experimental (circles and squares) and theoretical (lines) results for the basic phase control of the two-channel absorption in Na using the set of shaped pulses with the base phase patterns $\Phi_{\text{base}}(\omega)$ of a single π step. Shown are P_{4s} for the non-resonant two-photon absorption (squares and black line) and P_{7p} for the resonance-mediated (2+1) three-photon absorption (circles and gray line) as a function of the π -step position $\omega_{\text{step}}^{\text{base}}$. Each trace is normalized by the corresponding P_{4s} or P_{7p} excited by the TL pulse. The theoretical results are calculated numerically using Eqs.(1)-(5), using a grid with a bin size equal to the experimental shaping resolution $\delta\omega_{\text{shaping}}$. As can be seen, there is an excellent agreement between the experimental results and the numerical-theoretical results. The non-resonant two-photon absorption is controlled from zero to 100% of the absorption induced by the TL pulse [15]. The zero absorption corresponds to the two dark pulses occurring when $\omega_{\text{step}}^{\text{base}}=12896$ and 12844 cm^{-1} . Its upper limit is measured here to be 300-fold smaller than the TL absorption, as set by the best-achieved experimental noise. The resonance-mediated (2+1) three-photon absorption is experimentally controlled from 3% to 240% of the TL absorption [24]. The strong enhancement occurs when $\omega_{\text{step}}^{\text{base}}=\omega_{7p,4s}=12801 \text{ cm}^{-1}$. As previously identified [24], it originates from a change in the nature of the interferences between the positively-detuned ($\delta>0$) and negatively-detuned ($\delta<0$) near-resonant $3s$ - $7p$ three-photon pathways. With the TL pulse they are destructive, while with a π -step at $\omega_{7p,4s}$ they are constructive. Overall, as seen from the results, the π -step position simultaneously sets the two-photon and three-photon absorption levels to specific correlated values.

The implementation of the symmetry-based selective coherent control scheme presented above strongly reduces this correlation. Several examples are shown in Fig. 3. Each panel corresponds to a different position of the base π -step $\omega_{\text{step}}^{\text{base}}$ of $\Phi_{\text{base}}(\omega)$, setting the non-resonant two-photon absorption to a different chosen level ($P_{4s,\text{base}}$), as indicated in the panel's inset. The main graph in each panel displays the TL-normalized resonance-mediated (2+1) three-photon absorption (P_{7p}) resulting from different double-step anti-symmetric phase additions $\Delta\Phi_{\text{antisym}}(\omega)$ with $\Phi_{\text{amp}}^{\text{antisym}}=\pi$. It is presented as a function of the left π -step position $\omega_{\text{left-step},\pi}^{\text{antisym}}$. Shown are experimental (circles) and numerical-theoretical (lines) results.

Figure 3(a) shows the results for the case of zero two-photon absorption set by

$\omega_{\text{step}}^{\text{base}} = 12896 \text{ cm}^{-1}$. By scanning $\omega_{\text{left-step},\pi}^{\text{antisym}}$ across the spectrum, the three-photon absorption is continuously tuned experimentally from below 1% up to about 20% of the TL absorption, while the two-photon absorption is kept constant on its zero level that experimentally corresponds to a noise-level signal (see above). In other words, the results of Fig. 3(a) correspond to a family of shaped pulses that are all dark with respect to the two-photon absorption, while each of them induces a different three-photon absorption level tunable over an order-of-magnitude range of values. The present tuning range is determined only by the near-resonant component $A_{7p}^{(2+1)\text{near-res}}$ of the three-photon absorption amplitude, since a two-photon dark pulse also leads to a zero on-resonant component $A_{7p}^{(2+1)\text{on-res}}$ [see Eqs.(1)-(5)].

Figure 3(b) shows the results for the case of maximal two-photon absorption, i.e., the TL absorption. It is set by $\omega_{\text{step}}^{\text{base}}$ that is outside the spectrum, leading to a base phase pattern that is constant across the whole spectrum. By changing the π -step positions of the double-step anti-symmetric phase addition, the three-photon absorption is continuously tuned experimentally from $\sim 30\%$ up to $\sim 300\%$ of the TL absorption, while the two-photon absorption is kept constant on its maximal level. The strong enhancement of the resonance-mediated (2+1) three-photon absorption occurs when $\omega_{\text{left-step},\pi}^{\text{antisym}} = \omega_{7p,4s}$. The corresponding interference mechanism is similar to the one described above for the enhancement occurring with a single π -step at $\omega_{\text{step}}^{\text{base}} = \omega_{7p,4s}$: the introduction of such double anti-symmetric π -step leads to a destructive-to-constructive change in the nature of the interferences among near-resonant $3s$ - $7p$ three-photon pathways. The higher enhancement induced with the anti-symmetric double-step (300% vs. 240% of the TL absorption) is due to the fact that the anti-symmetric phase addition keeps the on-resonant component $A_{7p}^{(2+1)\text{on-res}}$ on its maximal magnitude set by the uniform base pattern, while a single π -step at $\omega_{\text{step}}^{\text{base}} = \omega_{7p,4s}$ sets it to a lower magnitude [24]. Figures 3(c)-(d) present additional selective control results where the two-photon absorption is set on constant intermediate levels in-between zero and the TL absorption, while the three-photon absorption is independently tuned experimentally from $\sim 10\%$ [Fig. 3(c)] or $\sim 20\%$ [Fig. 3(d)] up to $\sim 135\%$ of the TL absorption.

The complete picture for the extended selective femtosecond control of the two-channel absorption in Na is shown in Fig. 2(b), presenting numerical-theoretical results for the TL-normalized non-resonant two-photon absorption (P_{4s}) and resonance-mediated (2+1) three-photon absorption (P_{7p}). The two- and three-photon absorption levels set by a base π -step at a given $\omega_{\text{step}}^{\text{base}}$ are shown, respectively, by black and gray lines. These are the same theoretical

results shown in Fig. 2(a). The bar around each three-photon absorption point indicates the extended tuning range of the three-photon absorption achieved by applying all the possible double-step anti-symmetric phase additions of any $0-2\pi$ step amplitude $\Phi_{\text{amp}}^{\text{antisym}}$ and any steps' position (i.e., any $\omega_{\text{left-step}}^{\text{antisym}}$), while the two-photon absorption is kept constant on its corresponding base level (black line). As can be seen from this complete picture, for each two-photon absorption yield set by the base phase pattern, the three-photon absorption yield can independently be tuned over a range of values spanning one-two orders of magnitude. Hence, high degree of independent selective control is achieved among the two absorption channels and their degree of correlation is considerably reduced as compared to using only the base π -step patterns. Quantitatively, the base levels of the two- and three-photon absorption as well as the detuning range of the three-photon absorption depend on the spectral bandwidth of the pulse [24]. Still, qualitatively, comparable degree of high selectivity among the two channels is achieved with any spectral bandwidth.

In conclusion, we have introduced and demonstrated a new scheme for achieving high-degree of selective femtosecond coherent control among multiple excitation channels. The approach developed here is general, conceptually simple, and very effective. By proper pulse design, exploiting a symmetry property of one or more channels, the channels of symmetry are set constant on chosen yields while the other channels are tuned independently over a wide range of yields. When many channels are involved, the scheme can be applied iteratively to utilize different symmetry properties of different channels. Amplitude and polarization shaping [1] are natural extensions to the phase shaping employed here. Once corresponding symmetry properties are identified, the new scheme can be used in various multi-channel scenarios with various types of processes, including also photo-excitations that lead to ionization and/or dissociation.

This research was supported by The Israel Science Foundation (grant No. 127/02), by The James Franck Program in Laser Matter Interaction, and by The Technion's Fund for The Promotion of Research.

-
- [1] A. M. Weiner, Rev. Sci. Instr. **71**, 1929 (2000); T. Brixner and G. Gerber, Opt. Lett. **26**, 557 (2001); T. Brixner *et al.*, Appl. Phys. B **74**, S133 (2002).

- [2] D. J. Tannor, R. Kosloff, and S. A. Rice, *J. Chem. Phys.* **85**, 5805 (1986).
- [3] M. Shapiro and P. Brumer, *Principles of the quantum control of molecular processes* (Wiley, New Jersey, 2003).
- [4] W. S. Warren, H. Rabitz, and D. Mahleh, *Science* **259**, 1581 (1993).
- [5] H. Rabitz, R. de Vivie-Riedle, M. Motzkus, and K. Kompa, *Science* **288**, 824 (2000).
- [6] M. Dantus and V. V. Lozovoy, *Chem. Rev.* **104**, 1813 (2004); *ChemPhysChem* **6**, 1970 (2005).
- [7] R. Judson and H. Rabitz, *Phys. Rev. Lett.* **68**, 1500 (1992).
- [8] T. Brixner and G. Gerber, *ChemPhysChem* **4**, 418 (2003).
- [9] R. Levis, G. Menkir, and H. Rabitz, *Science* **292**, 709 (2001).
- [10] J. Herek *et al.*, *Nature (London)* **417**, 533 (2002).
- [11] N. Dudovich, D. Oron, and Y. Silberberg, *Phys. Rev. Lett.* **92**, 103003 (2004).
- [12] T. Baumert *et al.*, *Phys. Rev. Lett.* **67**, 3753 (1991).
- [13] D. Oron *et al.*, *Phys. Rev. A* **65**, 043408 (2002); N. Dudovich, D. Oron, and Y. Silberberg, *Nature (London)* **418**, 512 (2002); *J. Chem. Phys.* **118**, 9208 (2003).
- [14] M. Wollenhaupt *et al.*, *Phys. Rev. A* **68**, 015401 (2003); *Chem. Phys. Lett.* **419**, 184 (2006).
- [15] D. Meshulach and Y. Silberberg, *Nature (London)* **396**, 239 (1998); *Phys. Rev. A* **60**, 1287 (1999).
- [16] K. A. Walowicz *et al.*, *J. Phys. Chem. A* **106**, 9369 (2002); V. V. Lozovoy *et al.*, *J. Chem. Phys.* **118**, 3187 (2003).
- [17] A. Präkelt *et al.*, *Phys. Rev. A* **70**, 063407 (2004).
- [18] N. Dudovich *et al.*, *Phys. Rev. Lett.* **86**, 47 (2001).
- [19] B. Chatel, J. Degert, and B. Girard, *Phys. Rev. A* **70**, 053414 (2004).
- [20] P. Panek and A. Becker, *Phys. Rev. A* **74**, 023408 (2006).
- [21] E. Gershgoren *et al.*, *Opt. Lett.* **28**, 361 (2003).
- [22] H. U. Stauffer *et al.*, *J. Chem. Phys.* **116**, 946 (2002); X. Dai, E. W. Lerch, and S. R. Leone, *Phys. Rev. A* **73**, 023404 (2006).
- [23] S. Lim, A. G. Caster, and S. R. Leone, *Phys. Rev. A* **72**, 041803 (2005);
- [24] A. Gandman, L. Chuntunov, L. Rybak, and Z. Amitay, *Phys. Rev. A* **75**, 031401 (R) (2007); *Phys. Rev. A*, to be published (<http://arxiv.org/abs/0709.0601>).
- [25] L. Chuntunov, L. Rybak, A. Gandman, and Z. Amitay, <http://arxiv.org/abs/arXiv:0709.0486>; <http://arxiv.org/abs/arXiv:0709.0615>.

- [26] N. Dudovich *et al.*, Phys. Rev. Lett. **94**, 083002 (2005).
- [27] C. Trallero-Herrero *et al.*, Phys. Rev. Lett. **96**, 063603 (2006).
- [28] NIST Atomic Spectra Database (NIST, Gaithersburg, MD).

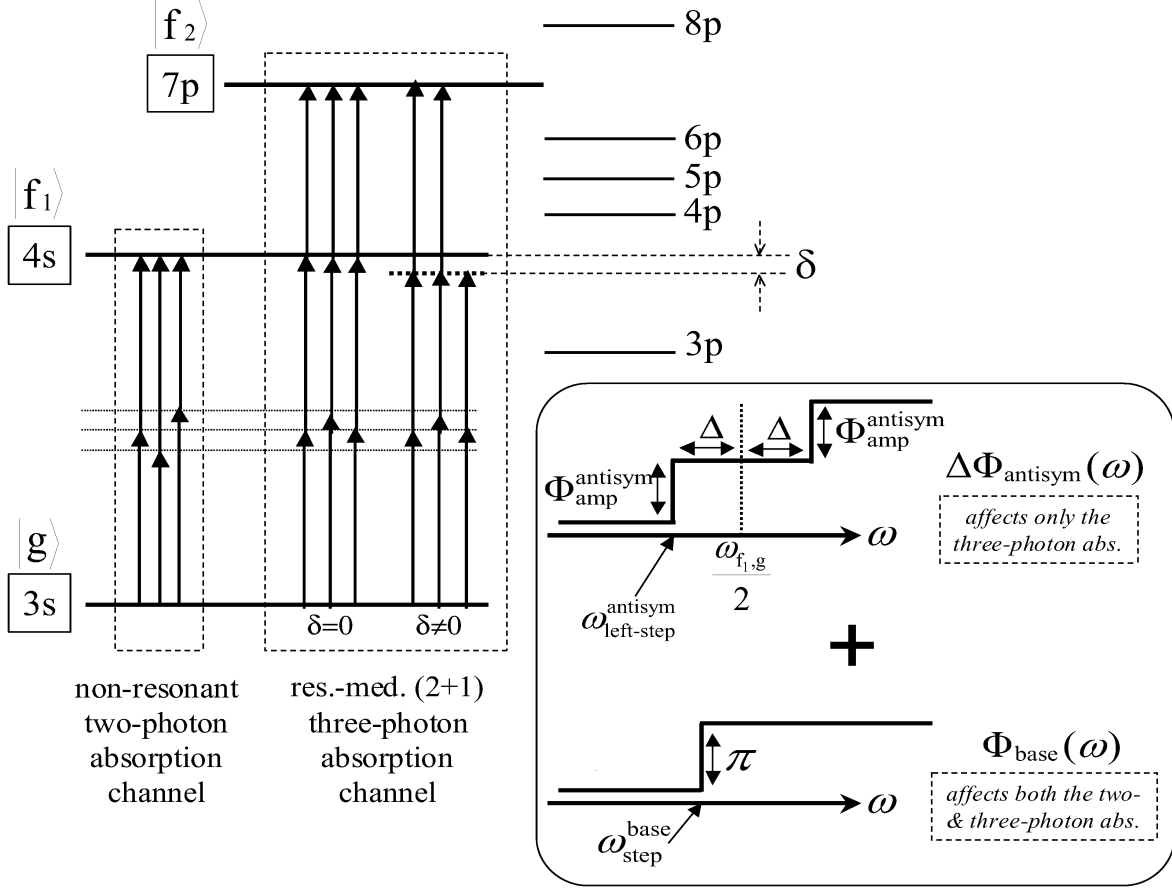


FIG. 1: The two-channel femtosecond excitation scheme of Na, including a non-resonant two-photon absorption channel from $|g\rangle \equiv 3s$ to $|f_1\rangle \equiv 4s$ and a resonance-mediated (2+1) three-photon absorption channel from $|g\rangle \equiv 3s$ to $|f_2\rangle \equiv 7p$ via $|f_1\rangle \equiv 4s$. Shown are examples of two- and three-photon pathways. The latter are either on resonance or near resonance with $|f_1\rangle$ (with detuning δ). The inset schematically shows the phase patterns used in the selective coherent control scheme. The base patterns $\Phi_{\text{base}}(\omega)$ are of a single π step at variable position $\omega_{\text{step}}^{\text{base}}$. The anti-symmetric additions $\Delta\Phi_{\text{antisym}}(\omega)$ are composed of two steps of variable amplitude $\Phi_{\text{amp}}^{\text{antisym}}$ positioned symmetrically around $\omega_{f_1,g}/2$ at variable positions that are represented by the left-step position $\omega_{\text{left-step}}^{\text{antisym}}$.

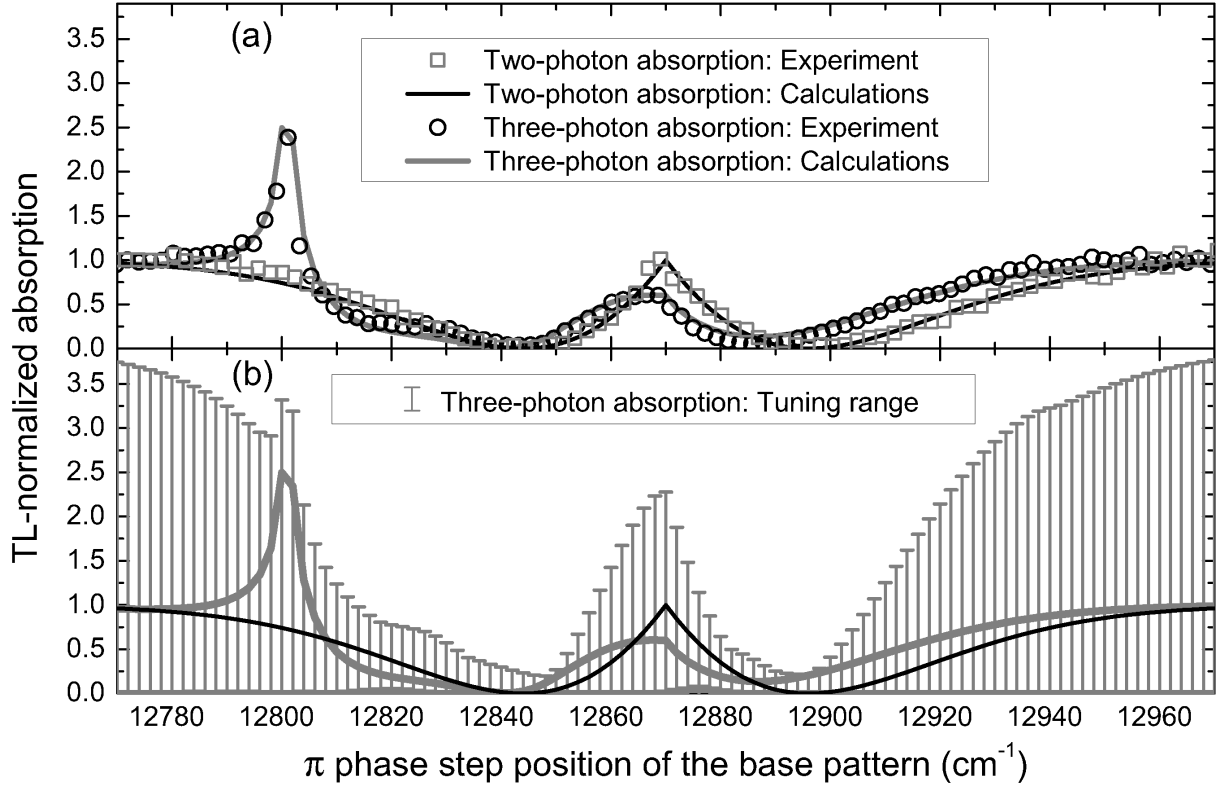


FIG. 2: (a) Experimental (circles and squares) and numerical-theoretical (lines) results for the TL-normalized non-resonant two-photon absorption (squares and black line) and resonance-mediated (2+1) three-photon absorption (circles and gray line) in Na, as a function of the π -step position $\omega_{\text{step}}^{\text{base}}$ of the base patterns $\Phi_{\text{base}}(\omega)$. (b) The complete picture of the extended symmetry-based selective control of the two-channel absorption in Na. The lines are the numerical-theoretical results for the two- and three-photon absorption set by the base phase patterns, presented also in panel (a). The bar around each three-photon absorption point indicates the extended tuning range of the three-photon absorption achieved by applying all the possible double-step anti-symmetric phase additions, while the two-photon absorption is kept constant on its corresponding base level.

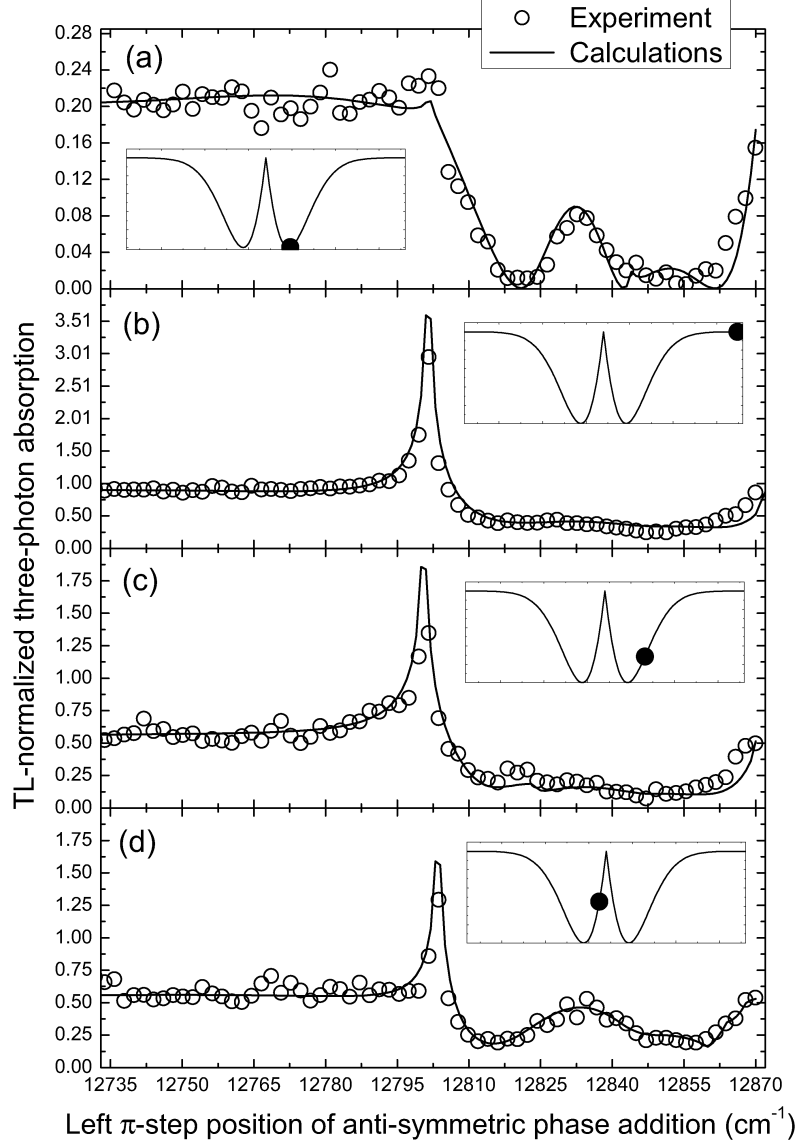


FIG. 3: Experimental (circles) and numerical-theoretical (lines) results for several example cases of the symmetry-based selective coherent control implementation. Each panel corresponds to a different position of the base π -step $\omega_{\text{step}}^{\text{base}}$ of $\Phi_{\text{base}}(\omega)$, setting the non-resonant two-photon absorption to a different chosen level indicated in the panel's inset. The main graph in each panel displays the TL-normalized resonance-mediated (2+1) three-photon absorption resulting from different anti-symmetric phase additions $\Delta\Phi_{\text{antisym}}(\omega)$ with a double π -step ($\Phi_{\text{amp}}^{\text{antisym}}=\pi$) at different positions represented by the left π -step position $\omega_{\text{left-step},\pi}^{\text{antisym}}$. The panels correspond to: (a) zero two-photon absorption, i.e., to a family of "two-photon dark pulses"; (b) maximal two-photon absorption, i.e., the TL absorption; and (c) and (d) intermediate levels of the two-photon absorption.